Available online at www.CivileJournal.org

Civil Engineering Journal

(E-ISSN: 2476-3055; ISSN: 2676-6957)

Vol. 12, No. 02, February, 2026

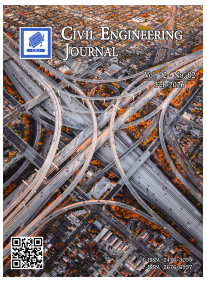

Comprehensive Characterization of Fly Ash as a Sustainable Supplementary Cementitious Material

Rizal Syahyadi [1, 2*], Taufiq Saidi [1, 3], Muttaqin Hasan [1, 3], Akhyar [1, 4], Amir Fauzi [2, 5], Aulia Rachman [5, 6]

[1] *Doctoral Program, School of Engineering, Post Graduate Program, Universitas Syiah Kuala, Acheh, 23111, Indonesia.*

[2] *Department of Civil Engineering, Politeknik Negeri Lhokseumawe, Acheh, 24375, Indonesia.*

[3] *Department of Civil Engineering, Universitas Syiah Kuala, Banda Aceh 23111, Indonesia.*

[4] *Department of Mechanical Engineering, Universitas Syiah Kuala, Banda Aceh 23111, Indonesia.*

[5] *Geopolymer and Green Technology Research Centre, Politeknik Negeri Lhokseumawe, Acheh, 24375, Indonesia.*

[6] *Department of Civil Engineering, Universitas Malikussaleh, Acheh, 24355, Indonesia.*

Received 24 August 2025; Revised 23 December 2025; Accepted 28 December 2025; Published 01 February 2026

Abstract

Sustainable development seeks to meet present needs without harming future generations. Rising energy demand from coal-fired power plants increases CO_2 emissions and produces fly ash (FA). The cement industry, responsible for about 7% of global CO_2 emissions, also consumes large amounts of energy. Incorporating FA as a partial or complete substitute for cement in concrete provided both environmental and performance advantages. Hence, this study focused on exploring the potential of FA from Nagan Raya (FANR) as a cementitious material for cement replacement. FANR was analyzed using XRF, XRD, FTIR, SEM, and EDS. It mainly contained SiO_2 (48.04%), Al_2O_3 (27.62%), and Fe_2O_3 (11.78%), meeting ASTM Class F fly ash standards. XRD analysis confirmed the presence of amorphous phases along with quartz and mullite crystals. FTIR showed silicate hydration products (C–S–H and C–A–H gels) at different water–cement ratios. SEM showed spherical particles with rough surfaces, which enhance reactivity but also increase water absorption and reduce workability. EDS confirmed silicate and aluminosilicate compositions. These results highlight FANR's potential as a sustainable cement replacement, despite workability issues.

Keywords: PCC Replacement; Material of FANR; XRF; XRD; FTIR; SEM/EDS.

1. Introduction

Sustainable development is currently a central issue in the modern world. As stated in the 1987 Bruntland Report, sustainable development must fulfill current demand without any trade-off affecting future generations' ability to accommodate their needs [1]. To achieve this target, there is a need for easy access to reliable and sustainable energy. The International Energy Agency (IEA) predicted a 5% increase in global power demand in 2021 and a 4% increase in 2022. In response to the rising demand, coal-based electricity production grew by more than 5% following a drop in 2020, with an additional 3% rise in 2022, potentially achieving a record peak [2]. This scenario triggered a substantial increase in the amount of fly ash (FA) waste from coal-fired power plants. However, FA can be used as an alternative material to replace cement in concrete mixtures.

* Corresponding author: rizal_syahyadi@pnl.ac.id

https://doi.org/10.28991/CEJ-2026-012-02-015

© 2026 by the authors. Licensee C.E.J, Tehran, Iran. This article is an open access article distributed under the terms and conditions of the Creative Commons Attribution (CC-BY) license (http://creativecommons.org/licenses/by/4.0/).

A total of 700 million tons of industrial byproducts impact the environment annually, with FA contributing a large volume [3, 4]. The application of FA in concrete reduces cement usage due to affordability and abundant availability, contributing to more sustainable waste management while reducing environmental pollution. This shows that FA has the potential to provide an alternative cement-binding material [5] and substantial benefits to concrete industry through two main methods. The first is the partial substitution of cement with FA due to pozzolanic properties. The second is the function of FA as a total cement replacement through the process of geopolymerization [6, 7]. The performance as a binding material greatly depends on several factors, including mineralogical composition, coal pulverization level, combustion setting, additives incorporated to optimize combustion or post-combustion reactions, and procedures for collecting, handling, and storing [8].

Fly ash (FA) is composed of fine, powdery particles, predominantly spherical in shape—either hollow or solid—with a glassy, porous texture. Its particles were smaller than 0.075 mm (No. 200 sieve), and the specific gravity ranged from 2.0 to 2.5, lower than that of cement. Its color ranges from black and gray to tan, depending on the amount of unburned carbon present. FA mainly contained quartz, mullite, and iron oxide, with silicon dioxide (SiO_2) as the primary component, making it suitable as a partial cement replacement in concrete. Fly ash was classified as Class C when the combined SiO_2, Al_2O_3, and Fe_2O_3 content was about 50–70%, while Class F contained over 70%. Class C also had over 18% calcium oxide (CaO), compared to less than 18% in Class F, which indicated Class C fly ash has more cementitious properties than Class F [9, 10].

Over the years, CANMET has studied the use of fly ash as a cement replacement, but the optimal substitution percentage remains undefined. CANMET's studies focused on high percentages of low-calcium fly ash (ASTM Class F) in concrete. Malhotra further analyzed these results through three tests, finding three key benefits: first, concrete with high low-calcium fly ash showed no expansion compared to control mixes with no ash; second, its dense structure made the concrete highly resistant to chloride ion penetration; and third, after undergoing six cycles of temperature changes (low to high) over 24 hours, the fly ash concrete demonstrated greater durability than conventional concrete [11].

Padhye & Deo [12] observed that most previous studies on fly ash focused on small replacement percentages with low-grade cement. To address this, they tested various fly ash proportions in high-grade concretes (M30, M40, M50) and examined their compressive strength over different curing periods. Their tests showed that increasing fly ash content reduced early strength compared to mixes without ash. They concluded that fly ash was a viable cement replacement as long as its content did not surpass 40%. Additionally, some mixtures with low proportions of high-grade cement and high fly ash content were more cost-effective than those mixed with low ash and low-grade cement [12].

The Nagan Raya Coal-Fired Power Plant in Aceh generates around 65 tons of fly ash daily, creating significant environmental concerns. This locally sourced material, known as Fly Ash Nagan Raya (FANR), was rich in silicon, iron, and aluminum, with distinct spherical particles featuring hazy surfaces. Unlike conventional fly ash, FANR exhibited features that raised water absorption and reduced concrete workability, highlighting the importance of further research on its properties and microstructural performance for use as a cement substitute [13, 14].

Guided by the sustainability framework in construction, this research emphasizes the use of industrial by-products to reduce reliance on ordinary Portland cement (OPC), a major contributor to CO_2 emissions. In this framework, FANR is examined as a partial replacement for cement, offering potential improvements in both mechanical and microstructural performance while advancing sustainable construction practices. The study applies advanced characterization techniques—XRF, XRD, SEM, FTIR, and EDS to examine FANR's conformity to pozzolanic reaction theory. Although previous studies on fly ash have noted both strengths and limitations, this study provides novelty by focusing on FANR, a locally available but underexplored material. By integrating theoretical insights with experimental results, it seeks to address research gaps and clarify FANR's potential contribution to sustainable construction.

2. Materials and Methods

2.1. FA

FA is a by-product material from coal combustion in the power plantation and commonly serves as a mineral admixture to enhance the properties of cement in concrete. Various factors influencing its characteristics include the type of coal used, the combustion environment, and the collection method [4, 15]. Applying FA in concrete contributes to the fresh and hardened concrete, enhancing workability, strength, and minimizing drying shrinkage [16–18]. Using FA in concrete also provides a solution to the storage and disposal issues associated with the industrial waste product.

2.2. Chemical Composition (XRF)

FA was typically classified based on the concentration of silicon (Si), iron (Fe), and aluminum (Al) in its composition. Generally, FA was categorized as a class C when the total amount of these elements exceeded 50%, while a class F contained more than 70% [15, 19]. Classification was also performed by calcium (Ca) composition, with low-Ca having 8-20 and high-Ca containing more than 20% [20]. Physically, FA consisted of spherical particles with an amorphous (glassy) structure and a diameter of less than 50 μm [21].

According to the ASTM C618 standard, FA contained a combination of glassy and crystalline phases, with typical ranges of SiO_2 (25–60%), Al_2O_3 (10–30%), and Fe_2O_3 (5–25%) [22]. These compositional characteristics were used to classify into Class C (CFA) and F (FFA), with the total content of SiO_2, Al_2O_3, and Fe_2O_3 required to be at least 50% for CFA and 70% for FFA [23]. Fauzi et al. (2016) found that the total amount of Si, Fe, and Al was 61.71% in class C and 91.35% in class F, respectively. Additionally, class C FA contained 27.1% CaO, and F had 1.32% CaO [24]. These compositional characteristics show that Class F was more pozzolanically reactive than Class C, showing suitability for application in concrete.

Rachman et al. (2021) conducted a study on Nagan Raya power plantation waste and found that FA was primarily composed of 37.16% Si and 17.61% Al, with a moderate Ca content of 8.72% [13]. This chemical composition provided a relatively stable setting time of approximately 4 to 5 hours. Isa et al. (2022) also emphasized that FA was classified as Class F when the sum of SiO_2, Al_2O_3, and Fe_2O_3 exceeded 70%, which enhanced pozzolanic activity [25]. During the reaction, the chemical content formed a gel of C-S-H and C-A-H, contributing to the mechanical properties. Komljenović et al. (2010) observed that FA had a high content of Si and Al but was low in CaO, favoring the formation of Si-O-Si, Si-O-Al, and N-A-S-H or C-A-S-H gel in alkali-based geopolymer systems [26].

Further results by Yaseen et al. (2023) stated that FA contained 35.73% SiO_2, 15.29% Al_2O_3, and 22.10% CaO, placing it compositionally between Class C and F [27]. Similarly, Jose et al. (2020) analyzed pond ash and recorded SiO_2, Al_2O_3, and CaO at 60.8% 23.9%, and 1.6%, respectively, reaffirming the classification as Class F [28]. The consistently high Si and Al content across these studies confirmed the potential of FA as a reactive pozzolanic material in cementitious systems [29].

2.3. XRD

Previous XRD examinations showed distinct diffraction patterns, presenting quartz (SiO_2) and mullite (Al_2O_3) as the primary crystalline phases in FA, while an amorphous background was in non-crystalline phases [30]. XRD patterns of FANR coal-fired power plant were predominantly inert or amorphous but reactive enough for the pozzolan reaction. Subsequently, the alkali activation decreased the intensity of crystalline peaks, which suggested a partial conversion of material into an amorphous gel phase [31, 32].

Isa et al. (2022) identified FA in the major crystalline components with quartz and mullite, while the presence of broad diffusing humps in XRD spectrum showed significant amorphous content [25]. The amorphous phase contributed to the high reactivity of material in cementitious systems, allowing for the gradual formation of secondary hydration products such as C–S–H and C–A–H gels [33]. Although Fauzi et al. (2016) did not provide full XRD data, the results showed that the presence of mullite and hematite was potentially reactive in pozzolanic interactions with alkaline activators [24].

The sharp peaks showed the crystalline components of quartz, mullite, calcined silica, and alumina [34]. These components played a role in the interaction with calcium hydroxide during hydration, contributing to the formation of hydration products that improved the microstructure of the composite material. Another study investigated further evidence of pozzolanic reactivity by examining XRD patterns of FA-blended cement. The results detected prominent crystalline peaks associated with portlandite ($Ca(OH)_2$), gypsum, ettringite, and calcium carbonate ($CaCO_3$) as hydration progressed [35]. The intensity peak of portlandite decreased with extended curing times, showing the gradual consumption of $Ca(OH)_2$ through pozzolanic reaction with FA. This reaction formed the C–S–H gel that enhanced the microstructure and mechanical strength of material [36]. Furthermore, XRD showed FA in the crystalline phases in quartz and mullite as a substantial amorphous fraction. The amorphous phase actively participated in pozzolanic reaction, leading to the formation of secondary hydration products that improved the strength, durability, and long-term performance of cementitious systems.

2.4. FTIR

Jose et al. (2020) reported that pond ash, chemically similar to Class F FA, showed distinct O–H stretching vibrations at 3456 cm^{-1} and Si–O vibrations in the range of 1034–1175 cm^{-1} [28]. Variations in the intensities of O–H and Si–O peaks during the hydration process showed the ongoing pozzolanic reactions and the gradual formation of C–S–H gel, which significantly enhanced the mechanical properties of material. Yaseen et al. (2023) also identified prominent Si–O stretching peaks at 953 cm^{-1} and Si–O bending peaks in the range of 410–445 cm^{-1} in the study of cement pastes blended with FA [37]. The increasing intensities of these peaks over curing periods of 90 days showed the continued formation of C–S–H as hydration progressed. Furthermore, an additional absorption peak at 3640 cm^{-1} was associated with the formation of portlandite ($Ca(OH)_2$). Mohanraj et al. (2020) observed a shift in the silicate vibration band (ν_3)

from approximately 920 cm^{-1} to 980 cm^{-1} in FA-blended cement composites over time [38]. This shift shows the progressive formation of secondary C–S–H gel. Additionally, the diminishing intensity of FA peak around 1096 cm-¹ serves as further confirmation of pozzolanic activity.

FTIR analyses consistently show that FA actively participates in pozzolanic reaction by contributing to the formation of C–S–H and C–A–H products. The key absorption bands commonly associated with pozzolanic activity include 450–470 cm^{-1} (Si–O–Si bending) and 980–1040 cm^{-1} (Si–O–Si and Si–O–Al stretching). Additionally, absorption bands observed at 1640–3460 cm^{-1} (O–H and H–O–H stretching and deformation) and 3690 cm^{-1} (O–H stretching from $Ca(OH)_2$) confirm the occurrence of hydration and pozzolanic reactions [28, 37, 38]. These spectral characteristics confirm that FA, particularly Class F, shows substantial potential as an active pozzolanic material, contributing to the mechanical properties and durability [39].

2.5. SEM and EDS

SEM observations across previous studies indicated that FA particles were predominantly spherical, with sizes ranging from the micro- to sub-micrometer scale and showing a variety of surface morphologies. The particle surface of FANR was misty, which increased the water absorption content in the fresh mixture and accelerated gel formation in the binder. However, the particles of FA were generally fine, spherical, and contained micropores that contributed to the formation of dense and compact concrete [13, 40, 41]. The use of SEM-EDS to examine elemental distribution showed the major elements such as Si, Al, Ca, and Fe across the particle surfaces [42, 43]. These morphological characteristics, particularly the smooth surface and rounded geometry, were significant because of the ability to improve the particle packing in fresh concrete mixtures, which reduced porosity and enhanced the mechanical properties [44, 45].

Fauzi et al. (2016) used EDS in conjunction with SEM, showing that the surface of FA was predominantly composed of Si, Al, and O, with smaller amounts of Ca and Fe [24]. This elemental composition suggested that FA was composed of amorphous aluminosilicate spheres, highly suitable for both hydration processes and pozzolanic activity. A high concentration of Si and Al reacted with Ca(OH)2, forming the gel of C–S–H and C-A-H that contributed directly to long-term strength development in cementitious systems [36, 46].

Further investigation showed the hydration progressed, and spherical FA particles became increasingly embedded within growing matrices of C–S–H and C–A–H (calcium aluminate hydrate) [47]. Over extended curing periods, most FA particles were partially or fully consumed in the hydration process, replaced by secondary products. Similarly, Mohanraj et al. (2020) observed that initially smooth particles gradually showed surface deterioration and fragmentation as hydration advanced. By 90 to 180 days, FA surfaces were integrated the gel of C–S–H reduced the overall porosity [38]. The results identified the formation of additional crystalline phases such as ettringite, gypsum, and Friedel's salt, particularly in areas exposed to aggressive environments, thereby enhancing the durability of the matrix. SEM–EDS analysis confirms that FA contributes to microstructural refinement and actively participates in pozzolanic reactions during hydration. The dissolution of FA particles into the gel of C–S–H and C–A–H improved the matrix density, reduced porosity, and enhanced the long-term strength as well as durability of cement-based composites.

2.6. Method and Experimental Works

This study used FA from the power plantation of Nagan Raya (FANR) in Aceh, Indonesia. Portland cement composite (PCC) was obtained from the market, and characterization was performed directly on material of FANR and PCC. Meanwhile, the microstructure of binder was investigated on normal and FANR concrete with the water-cement ratios of 0.55, 0.50, and 0.45, respectively [48]. This water-cement ratio was collected considering on the conventional and high performance mortar. The characteristics and microstructure were evaluated by using XRF to measure the chemical composition of material. XRD measured the mineralogical composition in the amorphous or crystalline phase, FTIR identified the chemical bonds, and SEM determined the morphology of material on surface texture, particle size, and particle shape [49].

The characteristics of PCC and FANR were measured using XRF, XRD, FTIR, SEM, and EDS. Furthermore, the fragment of concrete was prepared to measure the microstructure of the specimen. PCC, FANR, sand, and gravel were mixed in a drying condition. This was followed by pouring of water into the drying mix with the variations of water-cement ratios of 0.55, 0.50, and 0.45, respectively, to produce concrete as shown in Figure 1. Subsequently, concrete was cured for 28 days to achieve compressive strength and microstructure [48, 50]. The fragment obtained from the 28-day compressive strength was ground to form the smaller fraction and evaluated with XRD, FTIR, SEM, and EDS.

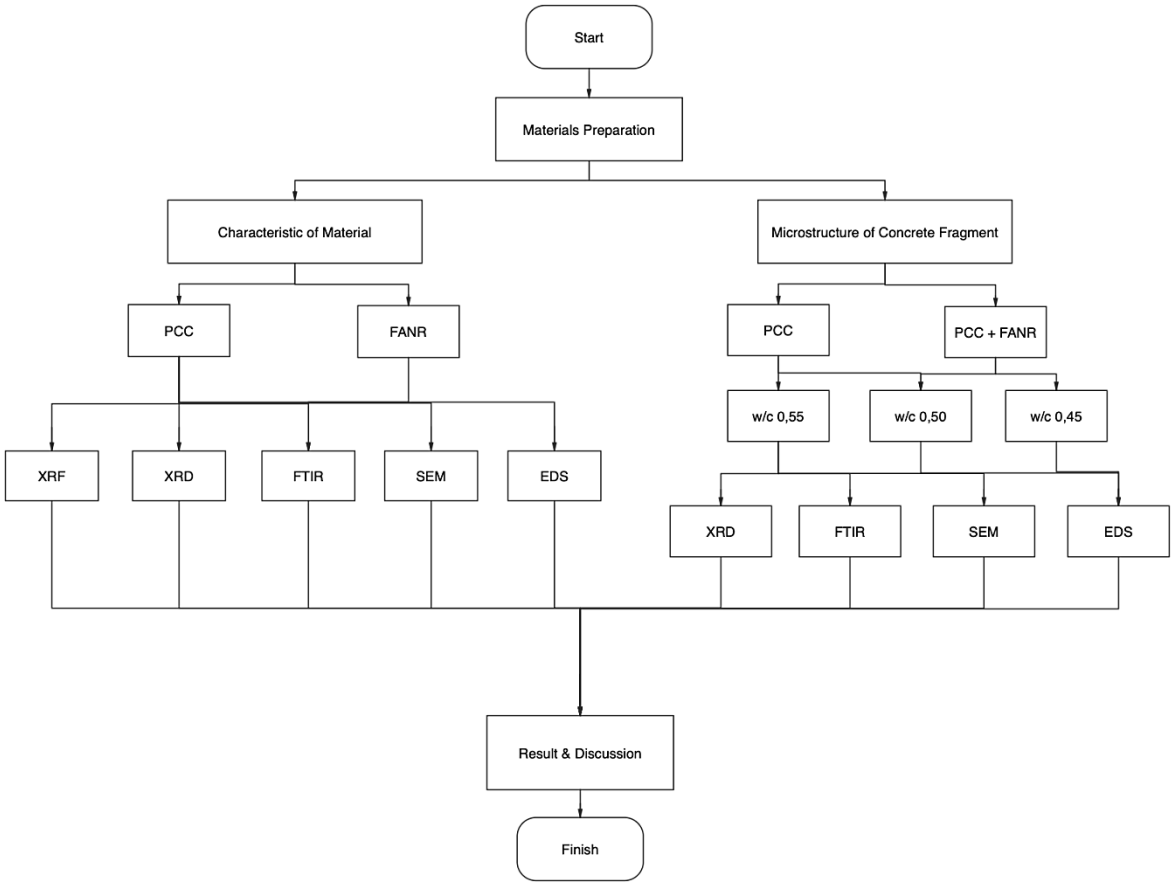

Figure 1. A schematic diagram to evaluate the characteristics and microstructure of FANR concrete fragments in the water-cement ratio of 0.55, 0.50, and 0.45, respectively

3. Results and Discussions

3.1. Chemical Composition of Material

Composite Cement (PCC). The results shows that FANR is primarily composed of SiO_2 (48.04%), Al_2O_3 (27.62%), and Fe_2O_3 (11.78%), which together account for approximately 87.44%. This percentage meets the minimum requirement for ASTM C618 Class F fly ash, confirming its classification as a low-calcium pozzolanic material. At approximately 6.44%, the CaO content of FANR is relatively minor, contrasting with PCC, where CaO constitutes 73.86% of the composition, accompanied by 14.22% SiO_2, 4.11% Al_2O_3, and 2.72% Fe_2O_3, as seen in Table 1.

Table 1. Chemical composition of PCC and FANR

Chemical composition in Oxide	Percentage weight	
	PCC	FANR
SiO_2	14.22	48.04
Al_2O_3	4.11	27.62
Fe_2O_3	2.72	11.78
CaO	73.86	6.44
MnO	0.09	0.21
K_2O	0.85	0.98
LOI	4.94	4.15

The high CaO content in PCC was crucial during hydration, where the initial reaction with water produced calcium silicate hydrate (C–S–H) gel and calcium hydroxide ($Ca(OH)_2$). The $Ca(OH)_2$ subsequently participated in secondary pozzolanic reactions with the silica and alumina from fly ash, leading to the formation of additional C–S–H and calcium aluminate hydrate (C–A–H) gels. These secondary reactions did not only densify the binder matrix but also significantly enhance the mechanical properties of concrete, particularly compressive strength. The availability of abundant calcium in PCC also accelerated early hydration, thereby contributing to the rapid development of early-age strength.

Aside from the dominant oxides, minor fractions of MnO, K_2O, and LOI are also identified in both FANR and PCC. Interestingly, the comparable LOI values suggests a similar amount of residual compounds or unburned carbon, a characteristic also noted in previous studies on fly ash sourced from coal-fired power plants. Studies by Ji et al. [51] and Alaj et al. [19] likewise showed that class F fly ash was mainly composed of Si, Al, and Fe oxides with low CaO content, and confirmed the importance of these oxides for sustaining long-term pozzolanic activity. These earlier findings support the present results, reinforcing the classification of FANR as a class F material with promising pozzolanic reactivity.

Overall, the comparison between FANR and PCC highlights the complementary nature of their chemical compositions. While PCC provides the high calcium content necessary for initial hydration and early strength development, FANR contributes reactive silica and alumina that engage in secondary pozzolanic reactions, further improving the durability and strength of the concrete matrix over time. These observations align with previous reports on the synergistic effect of blending low-calcium fly ash with cement, thereby validating the theoretical assumption that FANR has strong potential as a sustainable partial replacement for cement in concrete applications.

3.2. Identification of Material and Binder

Figure 2-a shows the XRD pattern of PCC, highlighting a dominant peak at approximately 2θ = 29.40°. Such a peak is characteristic of calcite ($CaCO_3$), which prior investigations documented as a significant crystalline component in Portland cement [52]. In addition, broad humps appear in the diffractogram, indicating the presence of a partially amorphous phase that was typical of cementitious binders. In comparison, FANR powder exhibited several distinct crystalline reflections, notably at 2θ = 26.6°, 20.9°, and 35.5°, which corresponds to quartz, mullite, and magnetite, respectively. Similar crystalline phases were identified in fly ash from various sources, with quartz and mullite being particularly common due to their high thermal stability [53, 54]. Alongside these crystalline constituents, FANR also displayed a considerable amorphous background, confirming its high hazy content, which was essential for pozzolanic activity.

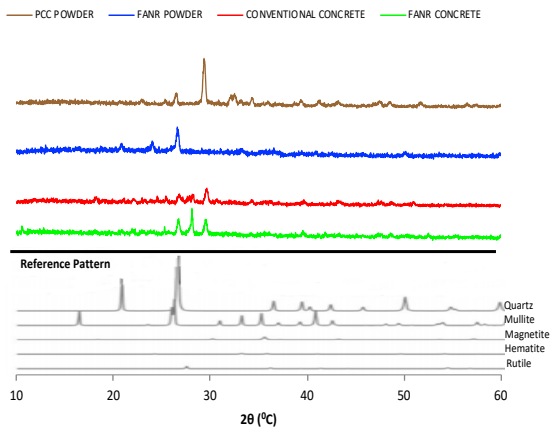

(a) XRD pattern in the w/c of 0.55

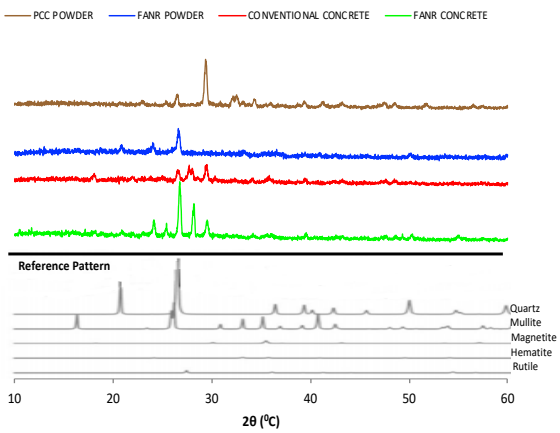

(b) XRD pattern in the w/c of 0.50

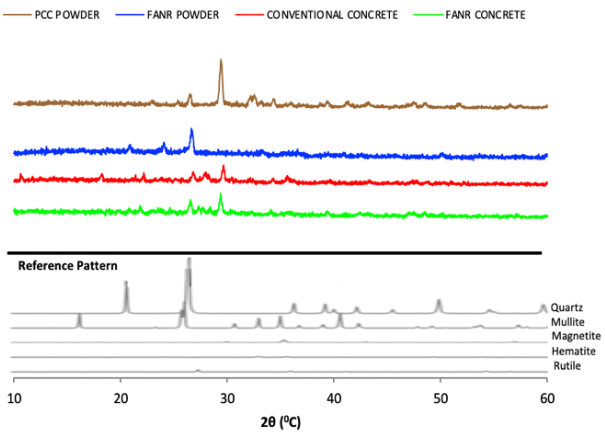

(c) XRD pattern in the w/c of 0.45

Figure 2. The identification of PCC, FANR, conventional concrete, and FANR concrete with the water-cement ratio of 0.55, 0.50, and 0.45

When incorporated into concrete, the XRD diffractogram of FANR showed broader and less intense peaks compared with the raw FANR powder. This reduction in intensity reflected the formation of hydration products, especially calcium silicate hydrate (C–S–H), which was known to be poorly crystalline in nature. Previous studies had similarly demonstrated that hydration of blended cementitious systems leads to the suppression of sharp crystalline peaks and the emergence of diffuse amorphous signals [55]. Interestingly, the diffraction peak at $2\theta = 26.6°$ in FANR concrete appeared sharper than that in conventional concrete, suggesting that the additional quartz supplied by fly ash increased the crystalline phase content. These observations corroborate earlier studies, which noted that quartz particles from fly ash persisted as crystalline remnants throughout extended hydration [56].

As depicted in Figure 2-b, the XRD results correspond to specimens produced at a water-to-cement ratio of 0.50. In this case, FANR retained the presence of quartz and mullite, along with a substantial amorphous fraction. The mineralogical profile of FANR concrete indicated that, although hydration products such as C–S–H and ettringite developed, crystalline residues from FA were still evident. These results suggests that the addition of FANR modified the mineralogical profile of the hydrated system through the presence of residual crystalline phases, consistent with findings from previous studies on class F fly ashes [57]. By contrast, the XRD pattern of conventional concrete with the same water-to-cement ratio displayed weaker peaks compared to both PCC and FANR. Such attenuation of crystalline peaks was associated with the dilution phenomenon and the transformation of hydration products into low-crystallinity phases, particularly C–S–H [55]. Compared with its conventional counterpart, FANR concrete produced broader diffuse peaks, which were indicative of a larger fraction of amorphous hydration phases, namely C–S–H and ettringite. This observation corroborated previous investigations indicating that FA contributed to the development of secondary C–S–H through its pozzolanic reactivity [57].

Figure 2-c illustrates the XRD patterns for a water-to-cement ratio of 0.45. At this ratio, conventional concrete showed reduced crystallinity compared with the raw cementitious materials, reflecting the dominance of amorphous hydration phases. FANR concrete, however, retained residual crystalline phases such as quartz and mullite. These remaining phases confirmed that the pozzolanic reaction of FA occurred partially but did not reach full completion within the experimental conditions. Such an observation is consistent with earlier reports indicating that quartz and mullite exhibited minimal reactivity during hydration and mainly served a filler role [57]. As a result, FANR played a dual role by generating amorphous gel phases through hydration and by incorporating stable crystalline residues into the concrete matrix. The presence of these crystalline residues in the XRD patterns provided evidence of incomplete pozzolanic reaction, which underscored the role of FANR as a supplementary cementitious material suitable for partial substitution rather than full replacement.

3.3. Bonding Identification of Material and binder

Figures 3-a to 3-c present the FTIR spectra of PCC, FANR, conventional concrete, and FANR concrete prepared with water-to-cement ratios of 0.55, 0.50, and 0.45, respectively. In Figure 3a, the FTIR spectrum is categorized into four areas, beginning with the range of ~3400 to 1600 cm^{-1}. This range corresponds to the water band, where a broad hump is typically associated with O–H stretching and bending vibrations arising from absorbed water or hydroxyl groups. Among the samples, FANR exhibits stronger signals in this region, suggesting higher hydroxyl or moisture content. This observation is consistent with earlier studies, which reported that the porous structure and reactive surface of fly ash enhance its water adsorption capacity [58].

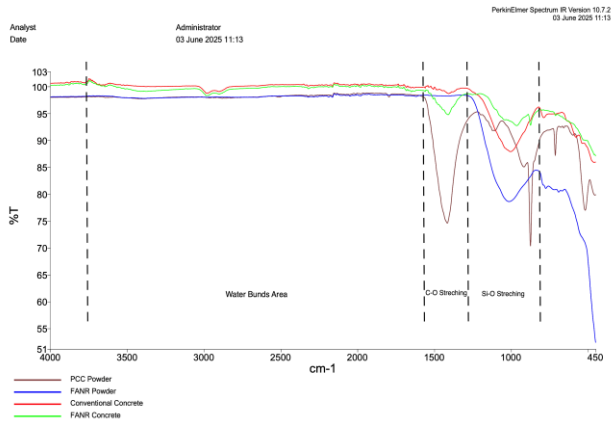

(a) FTIR in the w/c of 0.55

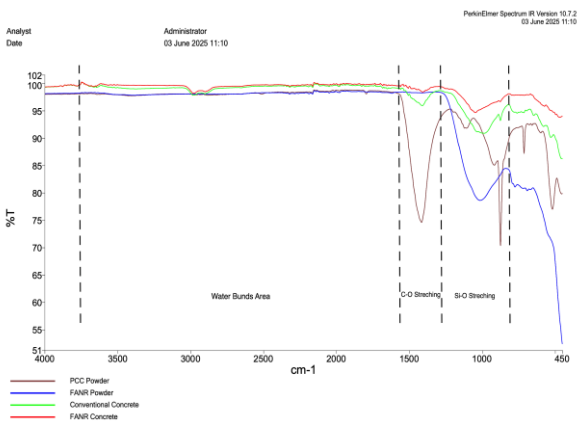

(b) FTIR in the w/c of 0.50

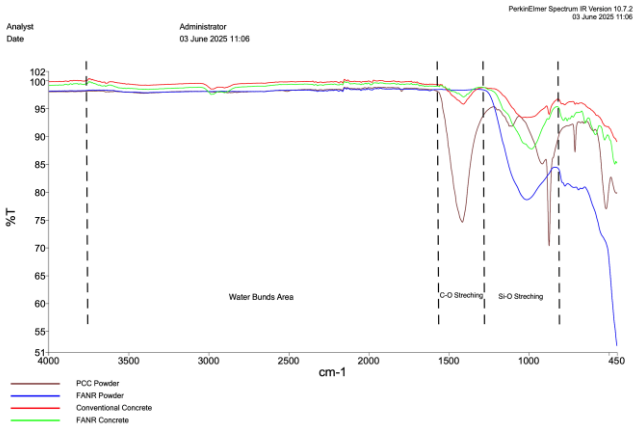

(c) FTIR in the w/c of 0.45

Figure 3. The bonding identification of PCC, FANR, conventional concrete, and FANR concrete with the water-cement ratio of 0.55, 0.50, and 0.45

The region between ~1400 and 1600 cm^{-1} displays absorption bands characteristic of C–O stretching, indicative of carbonate groups such as $CaCO_3$. A strong absorption in PCC confirms the presence of carbonate phases, while FANR produces a weaker signal, reflecting its relatively lower carbonate content. Previous research similarly demonstrated that Portland cement generally contains a higher level of carbonate minerals, which originate from clinker phases or secondary carbonation processes [58].

The spectral region spanning ~1400–450 cm^{-1} exhibits intense Si–O stretching absorptions, commonly associated with the vibrations of silicate frameworks. These absorptions were crucial for distinguishing alumino-silicate phases in fly ash as well as silicate-based hydration products in cement matrices, most notably calcium silicate hydrates (C–S–H). FANR displays prominent peaks in this region, confirming its alumino-silicate-rich composition. The spectral shifts observed between conventional concrete and FANR concrete indicated differences in the hydration products formed, highlighting the influence of FA addition on pozzolanic activity. Similar changes in silicate stretching vibrations have been reported in previous FTIR studies, indicating that the incorporation of fly ash alters the silicate network in hydration products [58, 59].

Figure 3-b presents the FTIR spectra for the water-to-cement ratio of 0.50, highlighting five distinct wavenumber regions. The broad hump observed between ~3400 and 3200 cm^{-1} again corresponds to O–H stretching vibrations, associated with hydroxyl groups. This band is present in all samples, confirming the presence of bound water. The region spanning ~3200 to 1650 cm^{-1} reflected H–O–H bending vibrations of water, with FANR concrete showing more pronounced signals. These observations suggest that FANR concrete exhibited a higher content of chemically and physically bound water. This finding aligns with earlier studies demonstrating that fly ash enhanced the water-retention capacity of cementitious systems, primarily due to its porous surface and fine particle size [58].

The absorption band near ~1450–1400 cm^{-1} corresponds to C–O stretching vibrations, representing carbonation products. PCC shows stronger absorption in this area, whereas FANR concrete displays weaker signals, reflecting differences in carbonate content. At ~1000–900 cm^{-1}, the spectra exhibit Si–O stretching bands, a critical region that reflects the structural vibrations of silicate phases. This spectral region corresponds to the development of calcium silicate hydrate (C–S–H), the principal hydration phase that governs the mechanical strength of cement-based materials. Earlier FTIR studies have similarly reported that the intensity and position of Si–O stretching bands shifted in blended systems with FA, reflecting ongoing pozzolanic reactions and secondary C–S–H formation [58].

The absorption bands at wavenumbers below 800 cm^{-1} represent Si–O bending vibrations and other mineral fingerprint regions. These bands provided additional evidence of silicate-rich phases and revealed differences in the extent of hydration or the presence of inert filler phases. The persistence of such signals in FANR concrete suggests that while hydration and pozzolanic reactions occurred, residual phases from fly ash remained in the matrix, in agreement with prior research noting the incomplete reactivity of quartz and mullite in Class F fly ash [58].

Figure 3-c presents the FTIR spectra obtained at a water-to-cement ratio of 0.45, which exhibit three distinct absorption regions, each offering valuable information on the bonding features within the system. The first region, located within 3700–3000 cm^{-1}, corresponds to the water bonding area. The broad band in this region corresponds to O–H stretching vibrations, commonly linked to molecular water or hydroxyl groups, confirming the presence of hydroxide phases in the samples. Similar broad O–H absorption bands have been observed in earlier FTIR studies of cementitious systems, attributed to both physically adsorbed water and chemically bonded hydroxyl groups in the hydration products [58, 59].

The second characteristic region, observed at approximately 1400–1500 cm^{-1}, represents the C–O stretching vibrations associated with carbonate (CO_3^{2-}) groups. These bands are indicative of calcite ($CaCO_3$) or carbonated cementitious phases, which arise either from intrinsic cement components or carbonation reactions during hydration. The strongest absorption signals in this region were observed in PCC powder and PCC concrete samples, highlighting the substantial formation of carbonate phases resulting from cement hydration. These findings are consistent with prior investigations, which reported carbonate absorptions as a characteristic component of Portland cement systems, especially when exposed to carbonation environments [58].

The third significant absorption region, located in the range of ~900–1100 cm^{-1}, is attributed to Si–O stretching vibrations, which are characteristic of silicate structures present in both raw materials and hydration products. This spectral region is of particular importance since it provides information on the underlying silicate framework, reflecting the structural features of both the raw materials and the hydration products that develop during cement hydration. Sharp and intense Si–O peaks in FANR powder and PCC powder indicate the presence of more crystalline and well-defined silicate structures, whereas the broader and less intense peaks observed in concrete specimens suggest overlapping contributions from the cementitious matrix and hydration products, particularly calcium silicate hydrate (C–S–H). Earlier FTIR analyses similarly reported broadening of the Si–O stretching bands in hydrated systems, attributing it to the formation of poorly crystalline C–S–H gels that dominated strength development [58].

In terms of comparative behavior, PCC powder displayed the sharpest and deepest silicate-related absorption peaks, consistent with its higher intrinsic silicate content. FANR powder, on the other hand, shows slight shifts in the Si–O bands, implying variations in mineralogical composition relative to PCC. FANR concrete exhibits stronger absorptions in the water and silicate regions, indicating heightened hydration activity, likely resulting from the pozzolanic reaction of FANR and the microstructure-modifying effects of its filler properties. In contrast, the spectral response of conventional concrete appears more closely aligned with that of PCC powder, indicating hydration dominated by typical cementitious phases without significant modification from supplementary materials. This behavior reflects findings in previous studies, where concretes incorporating fly ash showed distinguishable shifts and intensities in O–H and Si–O bands, confirming the dual role of fly ash as both a reactive pozzolanic material and an inert filler in cementitious systems [58-60].

3.4. Image of Material and Binder

Figure 4 illustrates the microstructural characteristics and elemental distribution of PCC, highlighting the fracture surface of the solid material. The micrographs reveal a heterogeneous texture composed of several distinct components, including large angular particles and a fine particulate matrix enveloping the coarser grains. PCC displays an overall morphology marked by a coarse surface texture and brittle fracture patterns, which are typical of ash-derived materials. The observed large angular particles correspond to common filler materials, previously reported as significant constituents of cementitious matrices [60, 61].

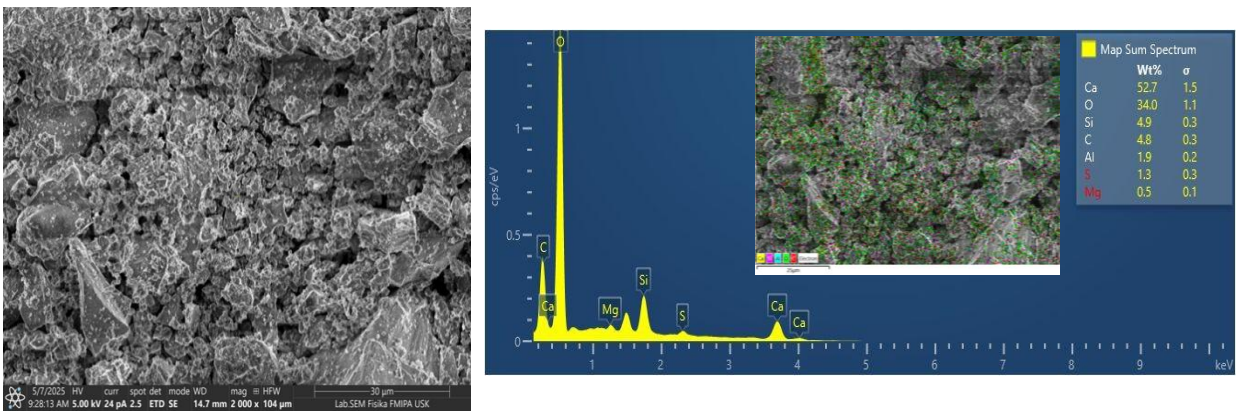

(a) SEM Image (b) Elemental distribution

Figure 4. The morphology characteristic of PCC

Elemental analysis further confirms the compositional characteristics of PCC. Calcium (Ca) and oxygen (O) appeared as the predominant elements in the spectrum, consistent with the calcium-based character of Portland cement and related materials. In addition to calcium and oxygen, silicon (Si) and sulfur (S) were identified in the spectrum, reflecting inputs from silicate-bearing minerals and gypsum, both of which are common constituents in Portland cement systems. These elemental constituents correspond to the raw materials commonly employed in Portland cement production, including limestone, gypsum, and other cementitious additives. Earlier studies similarly indicated that Portland cement mainly consists of calcium-containing phases, along with substantial silicates and minor sulfates, all of which were crucial for hydration and setting processes.

Figure 5 presents the particle morphology and elemental distribution of FANR, as revealed through SEM-EDS analysis. The micrographs demonstrate that FANR is composed predominantly of spherical and subspherical particles. Smooth, smaller spheres are regularly found on the surfaces of larger particles, accompanied by grain clusters that highlight their propensity to agglomerate. This morphology, characterized by spherical geometry and hazy surface texture, is indicative of the rapid cooling and solidification of molten material during fly ash formation, a feature commonly reported in previous studies on class F fly ash. The spherical shape was also known to confer high surface energy and improve particle packing, thereby impacting both the workability and pozzolanic reactivity of cementitious systems.

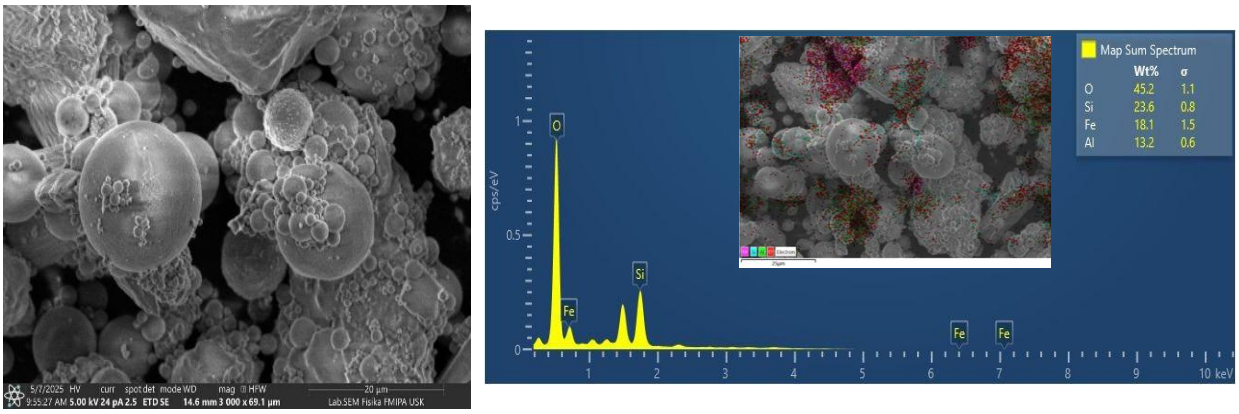

(a) SEM Image (b) Elemental distribution

Figure 5. The morphology characteristic of FANR

The EDS analysis further confirmed the chemical composition of FANR. Oxygen (O), aluminum (Al), and silicon (Si) are identified as the dominant elements, reflecting the presence of aluminosilicate phases, which are considered the primary reactive components of fly ash. These results are consistent with earlier reports, which noted that class F fly ashes typically consisted of a silica–alumina framework, making them suitable for pozzolanic applications in concrete. Moreover, the presence of iron (Fe) implied the existence of iron oxides—predominantly hematite or magnetite (Fe_2O_3/Fe_3O_4)—which was consistent with findings from previous characterizations of fly ash.

Figure 6 presents the microstructural features and elemental composition of conventional concrete prepared with a water-to-cement ratio of 0.55, as revealed by SEM-EDS analysis. The micrographs display a primary matrix dominated by sharp-edged and angular formations, characteristic of crystalline phases. The angular features developed into stacked plate-like layers, which were indicative of crystal growth and precipitation processes associated with cement hydration. In specific zones, the plate-like structures appeared disordered and gently curled, a morphology often associated with stress accumulation caused by crystal formation or by drying and shrinkage processes. Earlier investigations reported analogous structural characteristics, linking the presence of layered plate-like crystals to the formation of ettringite and secondary hydration phases in Portland cement.

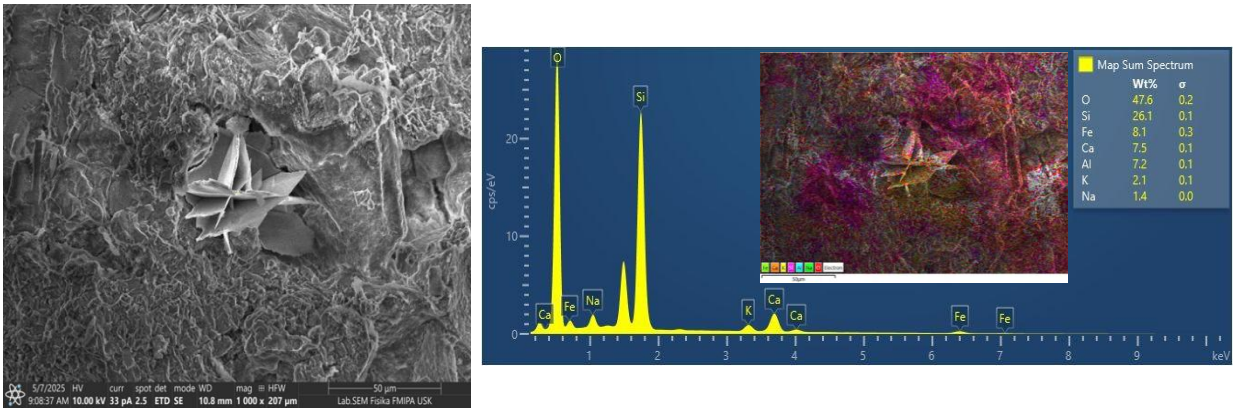

(a) SEM Image (b) Elemental distribution

Figure 6. The morphology characteristic of conventional concrete with the water-cement ratio of 0.55

The surrounding matrix exhibits rough, porous textures, suggestive of incomplete binder densification and indicative of the presence of ettringite or related crystalline hydrates. Earlier research likewise identified this type of porosity as a key attribute of traditional cement-based materials, where it played a crucial role in governing permeability and durability performance [61]. The inorganic crystalline nature of these features further pointed toward the precipitation of oxide phases, resulting from cement hydration and secondary reactions with additive materials. These results corroborated earlier findings that highlighted the contribution of supplementary phases to changes in hydration pathways and the subsequent formation of binding phases [61].

EDS analysis supports these morphological findings, with oxygen (O) and silicon (Si) identified as the dominant elements. This elemental composition is consistent with the presence of silicate minerals, most notably quartz, within the cementitious framework. Minor proportions of aluminum (Al) and sodium (Na) are also detected, suggesting the formation of aluminosilicate compounds, a feature that aligned with earlier characterizations of hydrated cementitious systems. Moreover, the detection of iron (Fe) indicates the potential formation of iron oxides, previously reported as accessory phases in concrete and linked to ceramic-like mineral assemblages [60]. Overall, the evidence suggests that the sample was primarily composed of silicate phases, complemented by oxide precipitates and crystalline hydration products, in agreement with previous investigations of the hydration chemistry and structural development of Portland cement–based concretes.

Figure 7 presents the microstructural features and elemental composition of FANR concrete prepared with a water-to-cement ratio of 0.55, as observed through SEM-EDS analysis. The central region of the micrograph reveals relatively flat, layered structures, indicative of crystalline formations typically associated with hydration products. Conversely, the upper-left region of the micrograph reveals fibrous or porous features, whereas the right-hand side shows clustered, rough, sponge-like textures that are indicative of amorphous phases. The distinct contrast between the compact, flat domains and the more porous clusters highlights the heterogeneity of the binder, suggesting differences in density and phase distribution. Such heterogeneous microstructures were typical of cementitious systems, where earlier studies reported the simultaneous presence of crystalline hydrates and amorphous gels.

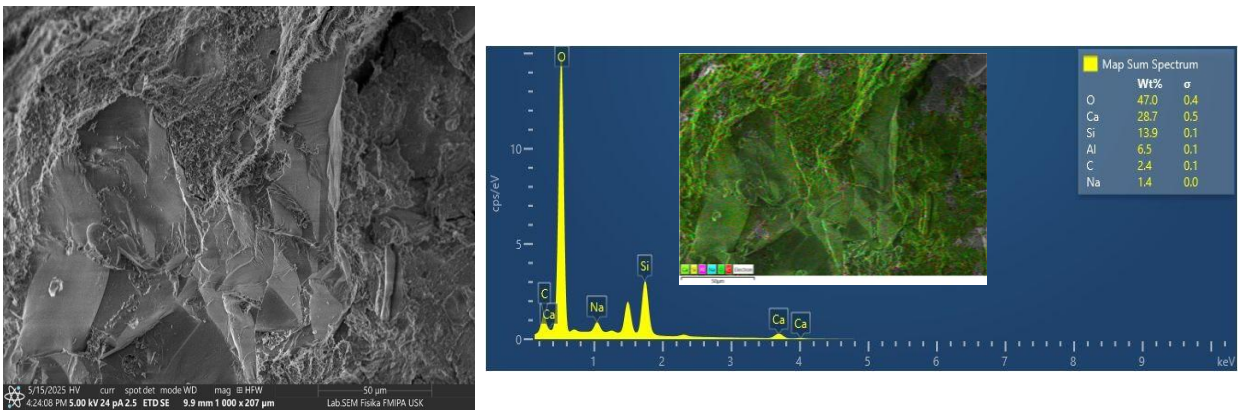

(a) SEM Image (a) Elemental distribution

Figure 7. The morphology characteristic of FANR concrete with the water-cement ratio of 0.55

EDS analysis further confirms the chemical composition of the FANR concrete matrix. Elevated O and Ca contents indicated the abundance of calcium-rich hydration products, primarily calcium silicate hydrates (C–S–H) and, in some cases, portlandite, consistent with typical Portland cement hydration chemistry. Moderate concentrations of Si are observed, consistent with contributions from fly ash–derived silicates. Consistent findings in the literature indicate that the coexistence of crystalline hydrates with amorphous aluminosilicate gels was a distinctive trait of fly incorporated concretes, directly linked to their strength evolution and durability performance.

Figure 8 illustrates the microstructural characteristics and elemental distribution of conventional concrete with a water-to-cement ratio of 0.50, as examined through SEM-EDS analysis. The image highlights four distinct surface morphologies. The central area shows a smooth, layered texture, typically associated with the crystallization processes that occur during cement hydration. By contrast, the left and right edges of the image display fibrous textures, which reflect surface irregularities arising from secondary hydration reactions. The middle-upper area exhibits a folded morphology, which indicates the entrapment of unreacted particles within the binder matrix. Earlier studies had similarly documented such heterogeneous surface characteristics, noting that the combination of smooth crystalline phases, fibrous ettringite-like structures, and porous regions was a typical feature of Portland cement–based systems.

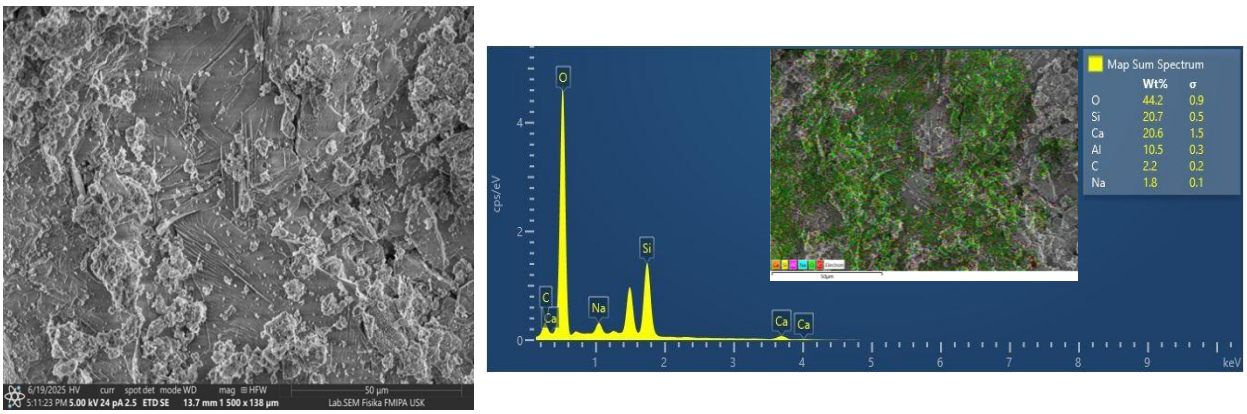

(a) SEM Image (b) Elemental distribution

Figure 8. The morphology characteristic of conventional concrete with the water-cement ratio of 0.50

EDS analysis of the focused area confirms the presence of elevated oxygen (O), silicon (Si), and calcium (Ca) contents. This elemental composition strongly suggested the occurrence of calcium silicate hydrates (C–S–H), silicate minerals, and other calcium-based crystalline phases, which were well-established as the primary hydration products of cement. Previous research on conventional concrete demonstrated comparable elemental distributions, where elevated concentrations of O, Si, and Ca were consistently associated with C–S–H gel and related cementitious phases, identified as key contributors to strength development and the stabilization of hydrated microstructures.

Figure 9 presents the SEM-EDS results of FANR concrete with a water-to-cement ratio of 0.50, highlighting both morphological and compositional characteristics. The micrograph reveals the presence of a distinct rectangular or cylindrical feature embedded within the fibrous binder matrix. Its smooth surface and sharply defined edges suggest that it acted as an additional component within the composite system, potentially functioning as a filler particle or reinforcing fiber. Surrounding this inclusion, the matrix was characterized by a complex network of fibrous and porous structures, displaying a rough and irregular texture. Such features reflected a high surface area and porosity, which were frequently associated with the heterogeneous hydration and pozzolanic reactions observed in fly ash–modified concretes.

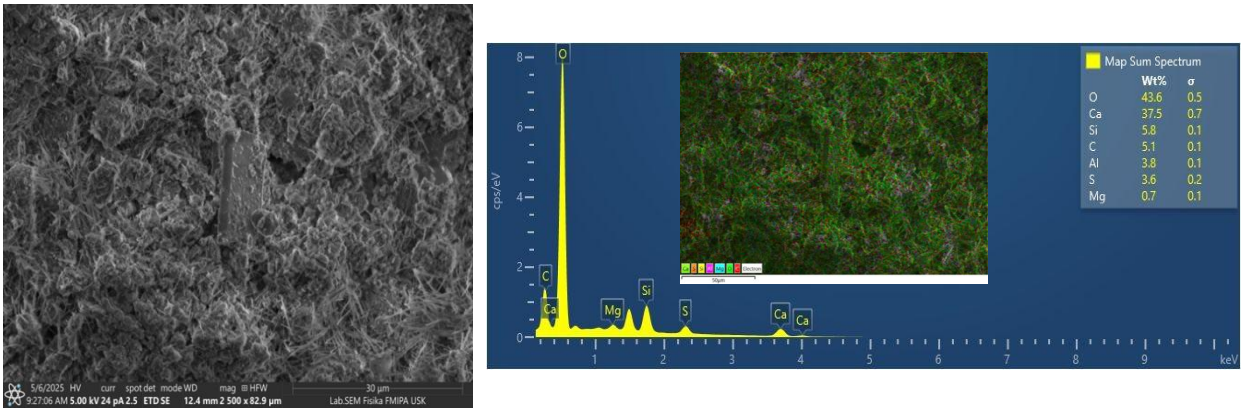

(a) SEM Image (b) Elemental distribution

Figure 9. The morphology characteristic of FANR concrete with the water-cement ratio of 0.50

According to the EDS analysis, the binder is predominantly composed of carbon (C) and oxygen (O), implying the occurrence of organic phases—an observation consistent with earlier reports on fly ash incorporated into cement-based materials. Furthermore, silicon (Si) and calcium (Ca) are identified as notable minor constituents, indicating the potential formation of silicate phases or calcium-bearing minerals such as $CaCO_3$ or $CaSiO_3$. These findings are consistent with earlier studies that documented the coexistence of amorphous carbon-rich domains, silicate phases, and calcium-bearing compounds as defining microstructural features of fly ash–blended concretes, all of which contributed to binder development, pore refinement, and long-term durability.

Figure 10 presents the SEM-EDS analysis of conventional concrete with a water-to-cement ratio of 0.45, highlighting notable microstructural and compositional features. The binder surface exhibits particles with flat, angular, and blade-shaped morphologies. The presence of smooth surfaces with sharply defined edges suggests that these features were not intrinsic to the hydrated cement matrix but rather correspond to unreacted particles originating from FANR. Previous studies similarly reported the occurrence of unreacted fly ash particles in blended concretes,

attributing this to incomplete hydration under certain curing conditions. In contrast, other binder areas show rough, porous textures, marking interfacial zones where phases meet and stresses concentrate. These heterogeneous microstructures were linked to transition zones between unreacted particles and the binder, influencing strength development and long-term durability.

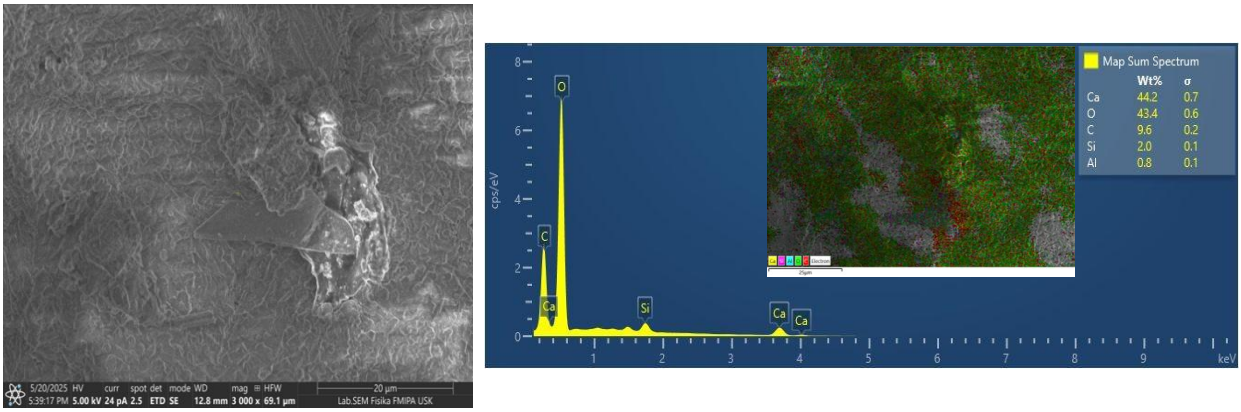

(a) SEM Image (b) Elemental distribution

Figure 10. The morphology characteristic of conventional concrete with the water-cement ratio of 0.45

EDS analysis identifies oxygen (O) and carbon (C) as the principal elements, suggesting the possible formation of carbonate compounds, which are commonly present in cementitious systems due to carbonation introduced by supplementary materials. Moreover, the detection of calcium (Ca) indicates the formation of calcium-based minerals, most likely calcium carbonate or hydration products such as portlandite, both of which were consistently reported in earlier studies examining the microstructural characteristics of conventional concrete.

Figure 11 presents the SEM-EDS results of FANR concrete with a water-to-cement ratio of 0.45, providing insight into its surface morphology and chemical composition. The micrograph reveals that the surface of the FANR concrete is predominantly rough, fibrous, and porous, which is characteristic of composite cementitious materials. The fibrous regions form a network of interconnected strands, indicative of a porous binder matrix that facilitated ion transport and contributed to the overall heterogeneity of the microstructure. In contrast, certain areas of the binder appear denser and smoother, suggesting the presence of unreacted particles embedded within the matrix. This feature is consistent with earlier studies on fly ash–blended concretes, where incomplete pozzolanic reaction resulted in the retention of unreacted particles within the hardened system.

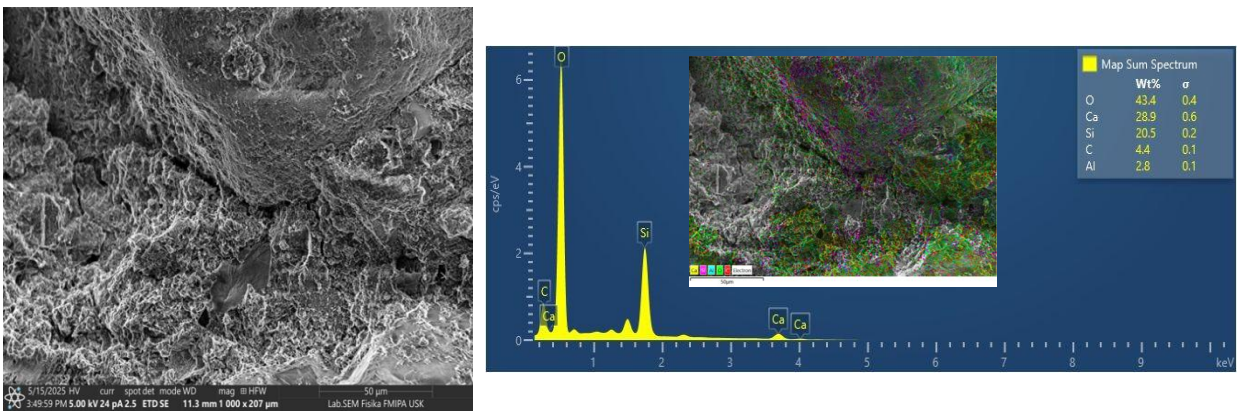

(a) SEM Image (b) Elemental distribution

Figure 11. The morphology characteristic of FANR concrete with the water-cement ratio of 0.45

The accompanying EDS analysis further supports these morphological observations. The investigated area reveals high concentrations of carbon (C) and calcium (Ca), indicating the presence of mineralized phases, likely in the form of calcium-rich hydrates such as calcium silicate hydrates (C–S–H). In addition, the detection of silicon (Si) and aluminum (Al) indicates the presence of ceramic-like aluminosilicate phases, which were typical of fly ash-derived components. These findings align with prior investigations, which reported that the coexistence of dense calcium-rich hydrates and amorphous aluminosilicate phases was a defining characteristic of fly ash–modified concretes, contributing not only to mechanical strength but also to long-term durability and microstructural refinement.

4. Conclusion

This study demonstrated the promising potential of FANR as a partial replacement for PCC in concrete, providing both chemical and microstructural enhancements to the cementitious matrix. XRF analysis indicated that FANR is rich in SiO_2, Al_2O_3, and Fe_2O_3, key components that support pozzolanic reactivity. Detailed phase analysis suggested that the presence of quartz and mullite in FANR contributed to an increased proportion of amorphous phases within the concrete, which was essential for promoting pozzolanic activity and enhancing the overall reactivity of the binder. FTIR spectroscopy further confirmed the existence of silicate and hydroxyl groups in FANR concrete, with stronger absorption observed in the water and silicate regions, indicating that the incorporation of FANR facilitated more advanced hydration reactions and a higher degree of interaction between fly ash particles and the cementitious phases.

Morphological and compositional investigations using SEM and EDS revealed that FANR particles were primarily spherical with a hazy surface, comprising significant amounts of Si, Al, and O, along with minor traces of Fe. These findings pointed to the presence of both aluminosilicate and ferrite phases, underscoring the intrinsic pozzolanic potential of FANR. Incorporating FANR into concrete was found to alter the hydration behavior and adjust the mineralogical makeup of the binder, resulting in improved mechanical strength and enhanced durability of the material. Overall, the study provided comprehensive evidence that FANR not only acted as a sustainable supplementary cementitious material but also enhanced the microstructural and mechanical characteristics of concrete, supporting its application in high-performance and durable cementitious systems.

5. Declarations

5.1. Author Contributions

Conceptualization, R.S. and A.F.; methodology, R.S. and A.F.; validation, T.S., M.H., A., and A.F.; formal analysis, R.S., T.S., M.H., and A.; investigation, R.S. and A.R.; resources, R.S.; data curation, R.S. and A.R.; writing—original draft preparation, R.S.; writing—review and editing, R.S. and A.R.; supervision, T.S., M.H., A., and A.F. All authors have read and agreed to the published version of the manuscript.

5.2. Data Availability Statement

The data presented in this study are available on request from the corresponding author.

5.3. Funding

The authors received no financial support for the research, authorship, and/or publication of this article.

5.4. Acknowledgments

The authors are grateful to the Department of Research and Development of Politeknik Negeri Lhokseumawe and Nagan Raya power plantation for their support.

5.5. Conflicts of Interest

The authors declare no conflict of interest.

6. References

[1] United Nations. (1987). Report of the World Commission on Environment and Development. United Nations, New York, United States

[2] Lorenczik, S., Zavala, P. B., & Hungerford, Z. (2021). Electricity Market Report. International Energy Agency (IEA), Paris, France.

[3] Nayak, D. K., Abhilash, P. P., Singh, R., Kumar, R., & Kumar, V. (2022). Fly ash for sustainable construction: A review of fly ash concrete and its beneficial use case studies. Cleaner Materials, 6, 1. doi:10.1016/j.clema.2022.100143.

[4] Filho, J. H., Medeiros, M. H. F., Pereira, E., Helene, P., & Isaia, G. C. (2013). High-Volume Fly Ash Concrete with and without Hydrated Lime: Chloride Diffusion Coefficient from Accelerated Test. Journal of Materials in Civil Engineering, 25(3), 411–418. doi:10.1061/(asce)mt.1943-5533.0000596.

[5] Alsharari, F. (2025). Utilization of industrial, agricultural, and construction waste in cementitious composites: A comprehensive review of their impact on concrete properties and sustainable construction practices. Materials Today Sustainability, 29. doi:10.1016/j.mtsust.2025.101080.

[6] Saingam, P., Chatveera, B., Promsawat, P., Hussain, Q., Nawaz, A., Makul, N., & Sua-Iam, G. (2024). Synergizing Portland Cement, high-volume fly ash and calcined calcium carbonate in producing self-compacting concrete: A comprehensive investigation of rheological, mechanical, and microstructural properties. Case Studies in Construction Materials, 21, e03832. doi:10.1016/j.cscm.2024.e03832.

[7] Saidi, T., & Hasan, M. (2022). The effect of partial replacement of cement with diatomaceous earth (DE) on the compressive strength and absorption of mortar. Journal of King Saud University - Engineering Sciences, 34(4), 250–259. doi:10.1016/j.jksues.2020.10.003.

[8] Diaz, E. I., Allouche, E. N., & Eklund, S. (2010). Factors affecting the suitability of fly ash as source material for geopolymers. Fuel, 89(5), 992–996. doi:10.1016/j.fuel.2009.09.012.

[9] Panda, L., & Dash, S. (2020). Characterization and utilization of coal fly ash: A review. Emerging Materials Research, 9(3), 921–934. doi:10.1680/jemmr.18.00097.

[10] Alterary, S. S., & Marei, N. H. (2021). Fly ash properties, characterization, and applications: A review. Journal of King Saud University - Science, 33(6). doi:10.1016/j.jksus.2021.101536.

[11] Antoni, A., Hartono, F., Tanuwijaya, S., Wijaya, K., Vianthi, A., & Hardjito, D. (2021). Comprehensive Investigation on the Potential of Fly Ash from New Source as Construction Material. Civil Engineering Dimension, 23(2), 78–90. doi:10.9744/ced.23.2.78-90.

[12] Padhye, R. D., & Deo, N. S. (2016). Cement replacement by fly ash in concrete. International Journal of Engineering Research, 5(1), 60-62.

[13] Rachman, A., Aulia, T. B., Fauzi, A., Syahyadi, R., Amalia, Z., & Rosnita, L. (2021). Feasibility of Nagan Raya Power Plantation Waste as Base Material on Geopolymer System. Key Engineering Materials, 876, 51–56. doi:10.4028/www.scientific.net/KEM.876.51.

[14] Ruhana, Fauzi, A., Syahyadi, R., Fajri, Rachman, A., Fazliah, Sumardi, & Mahyar, H. (2023). The influence of NaOh solution on the efflorescence of geopolymer mortar. The 2nd National Conference on Mathematics Education (NACOME-2021): Mathematical Proof as a Tool for Learning Mathematics, 2811, 070011. doi:10.1063/5.0117442.

[15] McCarthy, M. J., & Dyer, T. D. (2019). Pozzolanas and Pozzolanic Materials. Lea's Chemistry of Cement and Concrete, 363–467, Butterworth-Heinemann, Massachusetts, United States. doi:10.1016/B978-0-08-100773-0.00009-5.

[16] Saha, A. K. (2018). Effect of class F fly ash on the durability properties of concrete. Sustainable Environment Research, 28(1), 25–31. doi:10.1016/j.serj.2017.09.001.

[17] Rihan, M. A. M., Onchiri, R. O., Gathimba, N., & Sabuni, B. (2024). Mechanical and Microstructural Properties of Geopolymer Concrete Containing Fly Ash and Sugarcane Bagasse Ash. Civil Engineering Journal, 10(4), 1292–1309. doi:10.28991/CEJ-2024-010-04-018.

[18] Liu, Z., Takasu, K., Koyamada, H., & Suyama, H. (2022). A study on engineering properties and environmental impact of sustainable concrete with fly ash or GGBS. Construction and Building Materials, 316, 125776. doi:10.1016/j.conbuildmat.2021.125776.

[19] Alaj, A., Krelani, V., & Numao, T. (2023). Effect of Class F Fly Ash on Strength Properties of Concrete. Civil Engineering Journal (Iran), 9(9), 2249–2258. doi:10.28991/CEJ-2023-09-09-011.

[20] Altawil, H., & Olgun, M. (2025). Optimization of mechanical properties of geopolymer mortar based on Class C fly ash and silica fume: A Taguchi method approach. Case Studies in Construction Materials, 22, e04332. doi:10.1016/j.cscm.2025.e04332.

[21] Aydın, A. C., Nasl, V. J., & Kotan, T. (2018). The synergic influence of nano-silica and carbon nano tube on self-compacting concrete. Journal of Building Engineering, 20, 467–475. doi:10.1016/j.jobe.2018.08.013.

[22] ASTM C618-15. (2010). tandard Specification for Coal Fly Ash and Raw or Calcined Natural Pozzolan for Use in Concrete. ASTM International, Pennsylvania, United States. doi:10.1520/C0618-15 .

[23] Wang, Y. (2023). Reactivity and reactivity tests for unconventional fly ashes. Ph.D. Thesis, University of Miami, Coral Gables, United States.

[24] Fauzi, A., Nuruddin, M. F., Malkawi, A. B., & Abdullah, M. M. A. B. (2016). Study of Fly Ash Characterization as a Cementitious Material. Procedia Engineering, 148, 487–493. doi:10.1016/j.proeng.2016.06.535.

[25] Isa, F. N., Johari, M. A. M., Anum, I., Agabus, J. L., Soji, S. M., & Salihu, C. H. (2024). Performance of high strength concrete containing locust bean pod ash as cement replacement. Research on Engineering Structures and Materials, 10(1), 71–89. doi:10.17515/resm2023.837ma0802.

[26] Komljenović, M., Baščarević, Z., & Bradić, V. (2010). Mechanical and microstructural properties of alkali-activated fly ash geopolymers. Journal of Hazardous Materials, 181(1–3), 35–42. doi:10.1016/j.jhazmat.2010.04.064.

[27] Yaseen, N., Sahar, U., Bahrami, A., Mazhar Saleem, M., Ayyan Iqbal, M., & Saddique, I. (2023). Synergistic impacts of fly ash and sugarcane bagasse ash on performance of polyvinyl alcohol fiber-reinforced engineered cementitious composites. Results in Materials, 20. doi:10.1016/j.rinma.2023.100490.

[28] Jose, A., Nivitha, M. R., Krishnan, J. M., & Robinson, R. G. (2020). Characterization of cement stabilized pond ash using FTIR spectroscopy. Construction and Building Materials, 263. doi:10.1016/j.conbuildmat.2020.120136.

[29] Chindaprasirt, P., & Rukzon, S. (2008). Strength, porosity and corrosion resistance of ternary blend Portland cement, Rice husk ash and fly ash mortar. Construction and Building Materials, 22(8), 1601-1606. doi:10.1016/j.conbuildmat.2007.06.010.

[30] van Riessen, A., Jamieson, E., Gildenhuys, H., Skane, R., & Allery, J. (2025). Using XRD to Assess the Strength of Fly-Ash- and Metakaolin-Based Geopolymers. Materials, 18(9), 1. doi:10.3390/ma18092093.

[31] Nurmalita, N., Madjid, S. N., Setiawan, A., Idroes, R., & Jalil, Z. (2023). Characteristics of Silica Powder Extracted from Fly Ash of Coal Fired Power Plant – Effect of Heat Treatment Process. Journal of Ecological Engineering, 24(9), 282–292. doi:10.12911/22998993/169289.

[32] Petrus, H. T. B. M., Olvianas, M., Suprapta, W., Setiawan, F. A., Prasetya, A., Sutijan, & Anggara, F. (2020). Cenospheres characterization from Indonesian coal-fired power plant fly ash and their potential utilization. Journal of Environmental Chemical Engineering, 8(5). doi:10.1016/j.jece.2020.104116.

[33] Reig, L., Sanz, M. A., Borrachero, M. V., Monzó, J., Soriano, L., & Payá, J. O. R. D. I. (2017). Compressive strength and microstructure of alkali-activated mortars with high ceramic waste content. Ceramics International, 43(16), 13622-13634. doi:10.1016/j.ceramint.2017.07.072.

[34] Aripin, H., Mitsudo, S., Prima, E. S., Sudiana, I. N., Kikuchi, H., Sano, S., & Sabchevski, S. (2015). Crystalline mullite formation from mixtures of alumina and a novel material - Silica xerogel converted from sago waste ash. Ceramics International, 41(5), 6488–6497. doi:10.1016/j.ceramint.2015.01.092.

[35] Steiner, S., Lothenbach, B., Proske, T., Borgschulte, A., & Winnefeld, F. (2020). Effect of relative humidity on the carbonation rate of portlandite, calcium silicate hydrates and ettringite. Cement and Concrete Research, 135. doi:10.1016/j.cemconres.2020.106116.

[36] Lee, H. J., Lee, J. H., & Kim, D. G. (2012). Study on the change in microstructure of Fly ash concrete depending on ages and degree of hydration using XRD and SEM. Advanced Materials Research, 486, 350–355. doi:10.4028/www.scientific.net/AMR.486.350.

[37] Yaseen, S. A., Yiseen, G. A., Poon, C. S., Leung, C. K., & Li, Z. (2023). The effectuation of seawater on the microstructural features and the compressive strength of fly ash blended cement at early and later ages. Journal of the American Ceramic Society, 106(8), 4967–4986. doi:10.1111/jace.19109.

[38] Mohanraj, K., Sivakumar, G., & Barathan, S. (2010). Hydration Process of Fly Ash Blended Cement Composite. International Journal of Chemical Sciences, 8(1), 589-601.

[39] Karamyan, H., Avagyan, M., Shainova, R., Sahakyan, A., Baghdagyulyan, A., Tepanosyan, G., … Badalyan , M. (2025). Combined Effect of Basalt Fibers and Bentonite Clay on Complex Mortar Properties. Civil Engineering Journal, 11(12), 5006–5018. Doi:10.28991/CEJ-2025-011-12-05.

[40] Kutchko, B. G., & Kim, A. G. (2006). Fly ash characterization by SEM-EDS. Fuel, 85(17–18), 2537–2544. doi:10.1016/j.fuel.2006.05.016.

[41] Younes, M. M., Abdel-Rahman, H. A., & Khattab, M. M. (2018). Utilization of rice husk ash and waste glass in the production of ternary blended cement mortar composites. Journal of Building Engineering, 20, 42-50. doi:10.1016/j.jobe.2018.07.001.

[42] Piispanen, M. H., Arvilommi, S. A., Broeck, B. V. D., Nuutinen, L. H., Tiainen, M. S., Peramaki, P. J., & Laitinen, R. S. (2009). A comparative study of fly ash characterization by LA-ICP-MS and SEM-EDS. Energy & Fuels, 23(7), 3451-3456. doi:10.1016/j.jhazmat.2008.05.029.

[43] Aulia, T. B., Muttaqin, M., Afifuddin, M., Zaki, M., & Firdaus. (2020). Effect of utilizing geopolymer fly ash on potential and corrosion rate of reinforcement in high-strength concrete. IOP Conference Series: Materials Science and Engineering, 933(1), 012047. doi:10.1088/1757-899X/933/1/012047.

[44] Ren, G., Tian, Z., Wu, J., & Gao, X. (2021). Effects of combined accelerating admixtures on mechanical strength and microstructure of cement mortar. Construction and Building Materials, 304, 124642. doi:10.1016/j.conbuildmat.2021.124642.

[45] Yurdakul, E., Taylor, P. C., Ceylan, H., & Bektas, F. (2014). Effect of Water-to-Binder Ratio, Air Content, and Type of Cementitious Materials on Fresh and Hardened Properties of Binary and Ternary Blended Concrete. Journal of Materials in Civil Engineering, 26(6), 1. doi:10.1061/(asce)mt.1943-5533.0000900.

[46] Nath, P., & Sarker, P. (2011). Effect of Fly Ash on the Durability Properties of High Strength Concrete. Procedia Engineering, 14, 1149–1156. doi:10.1016/j.proeng.2011.07.144.

[47] Shahsavari, R., & Hwang, S. H. (2018). Morphogenesis of Cement Hydrate: From Natural C-S-H to Synthetic C-S-H. Cement Based Materials. doi:10.5772/intechopen.77723.

[48] Tauqir, A. (2018). Determination of water/cement-ratio of cement. Master Thesis, Aalto University, Helsinki, Finland.

[49] Chintalapudi, K., & Pannem, R. M. R. (2020). The effects of Graphene Oxide addition on hydration process, crystal shapes, and microstructural transformation of Ordinary Portland Cement. Journal of Building Engineering, 32. doi:10.1016/j.jobe.2020.101551.

[50] Wang, G., Kong, Y., Sun, T., & Shui, Z. (2013). Effect of water-binder ratio and fly ash on the homogeneity of concrete. Construction and Building Materials, 38, 1129–1134. doi:10.1016/j.conbuildmat.2012.09.027.

[51] Ji, X., Zhang, C., Yang, Y., Zhang, J., Tang, L., & Ji, D. (2025). A New Classification Method for High-Volume Fly Ash: Performance Based on Coal Source and Particle Size. Materials, 18(17). doi:10.3390/ma18174145.

[52] Jhatial, A. A., Nováková, I., Gjerløw, E., & Engelsen, C. J. (2025). Preliminary characterization and evaluation of local concrete sludges for use as supplementary cementitious materials. In Case Studies in Construction Materials (Vol. 22). doi:10.1016/j.cscm.2025.e04319.

[53] Javed, U., Shaikh, F. U. A., & Sarker, P. K. (2024). Thermal stability and strength degradation of lithium slag geopolymer containing fly ash and silica fume. Construction and Building Materials, 425. doi:10.1016/j.conbuildmat.2024.135976.

[54] Yu, Y., Gunasekara, C., Elakneswaran, Y., Robert, D., Law, D. W., & Setunge, S. (2025). Influence of amorphous content in recycled fly ash on binder hydration characteristics. Journal of Material Cycles and Waste Management, 27(2), 729–745. doi:10.1007/s10163-024-02147-7.

[55] Jwaida, Z., Jadooe, A., Dulaimi, A., Almuhanna, R. R. A., Hawesah, H. Al, Bernardo, L. F. A., & Andrade, J. M. de A. (2025). Investigating the Properties of Composite Cement-Based Mortar Containing High Volumes of GGBS and CCR. Journal of Composites Science, 9(6). doi:10.3390/jcs9060301.

[56] Chen, X. F., Zhang, X. C., & Peng, Y. (2025). Multi-Scale Investigation of Fly Ash Aggregates (FAAs) in Concrete: From Macroscopic Physical–Mechanical Properties to Microscopic Structure of Hydration Products. Materials, 18(11). doi:10.3390/ma18112651.

[57] Qu, B., Martin, A., Pastor, J. Y., Palomo, A., & Fernández Jiménez, A. (2022). Effects of elevated temperatures on properties of hybrid alkaline-belite cement with high level of fly ash. Journal of Materials Research and Technology, 21, 2455–2470. doi:10.1016/j.jmrt.2022.10.084.

[58] Dai, F., Zhuang, Q., Huang, G., Deng, H., & Zhang, X. (2023). Infrared Spectrum Characteristics and Quantification of OH Groups in Coal. ACS Omega, 8(19), 17064–17076. doi:10.1021/acsomega.3c01336.

[59] Pasieczna-Patkowska, S., Cichy, M., & Flieger, J. (2025). Application of Fourier Transform Infrared (FTIR) Spectroscopy in Characterization of Green Synthesized Nanoparticles. Molecules, 30(3). doi:10.3390/molecules30030684.

[60] Mehta, P. K. & Monteiro, P. J. M. (2006) Concrete: Microstructure, Properties, and Materials (3rd Ed.). McGraw-Hill, Columbus, United States.

[61] Kupwade-Patil, K., Al-Aibani, A. F., Abdulsalam, M. F., Mao, C., Bumajdad, A., Palkovic, S. D., & Büyüköztürk, O. (2016). Microstructure of cement paste with natural pozzolanic volcanic ash and Portland cement at different stages of curing. Construction and Building Materials, 113, 423–441. doi:10.1016/j.conbuildmat.2016.03.084.